

FULL PAPER

# Photoluminescence of perovskite-type $\text{Cr}^{3+}$ -activated phosphors in the La–Al–Ti–O system

Akihiro Nakanishi<sup>1,†</sup>, Takayuki Nakanishi<sup>1</sup>, Naoto Hirosaki<sup>1</sup>, Koji Morita<sup>2</sup> and Takashi Takeda<sup>1,‡</sup>

<sup>1</sup>Advanced Phosphor Group, National Institute for Materials Science, Tsukuba, Ibaraki 305–0044, Japan

<sup>2</sup>Polycrystalline Optical Material Group, National Institute for Materials Science, Tsukuba, Ibaraki 305–0044, Japan

$\text{Cr}^{3+}$ -activated near-infrared emitting phosphor has a potential application in plant growth and sensing technologies. Herein, we synthesized near-infrared emitting  $\text{La}_{1-x/3}\text{Al}_{1-x-y}\text{Ti}_x\text{O}_3:y\text{Cr}^{3+}$  phosphor by a solid-state reaction.  $\text{La}_{1-x/3}\text{Al}_{1-x-y}\text{Ti}_x\text{O}_3:y\text{Cr}^{3+}$  ( $x = 0.2$ ,  $y = 0.003$ ) showed the near-infrared emission at 751 nm with a full width at half-maximum of 41 nm under 351 nm excitation. The internal and external quantum efficiencies were 54.4 and 25.5 %, respectively. The luminescence intensities at 150 °C of the  $\text{La}_{1-x/3}\text{Al}_{1-x-y}\text{Ti}_x\text{O}_3:y\text{Cr}^{3+}$  ( $x = 0.1$ , 0.2, and 0.3,  $y = 0.003$ ) were 32, 17, and 3 % of those at room temperature, respectively. The thermal quenching effect strongly occurred with increasing the amount of Ti and it was related to the change in the absorbance edge of the host material  $\text{La}_{1-x/3}\text{Al}_{1-x-y}\text{Ti}_x\text{O}_3$ .

Key-words :  $\text{Cr}^{3+}$ -activated phosphor, Near-infrared emission, Oxide, Solid state reaction

[Received November 26, 2025; Accepted December 23, 2025; Published online February 3, 2026]

## 1. Introduction

White LEDs combined with blue or ultraviolet LED and phosphors are widely used because of high efficiency and long life.<sup>1–3)</sup> Yellow- [ $\text{Y}_3\text{Al}_5\text{O}_{12}:\text{Ce}^{3+}$  and  $\text{Ca-}\alpha\text{-SiAlON}$  ( $\text{Ca}_{m/2}\text{Si}_{12-m-n}\text{Al}_{m+n}\text{O}_n\text{N}_{16-n}:\text{Eu}^{2+}$ )], and red- [ $\text{CaAlSiN}_3:\text{Eu}^{2+}$  and  $\text{M}_2\text{Si}_5\text{N}_8:\text{Eu}^{2+}$  ( $\text{M} = \text{Ca}, \text{Sr}$ )] emitting phosphors are commercially utilized for white LEDs.<sup>4–8)</sup>

Near-infrared (NIR) light sources have been applied in various agricultural technologies, including plant growth and sensing systems.<sup>9–11)</sup> The height and growth of plants is controlled by adjusting the ratio of red to near-infrared light irradiation, owing to the strong absorption of biological pigments such as red-absorbing phytochrome ( $\text{P}_R$ ) and far-red-absorbing phytochrome ( $\text{P}_{FR}$ ).<sup>12)</sup> In addition, the reflectance difference between live and dead leaves is widely utilized for assessing plant health and evaluating vegetation. Plants exhibit high reflectance at  $\sim 750\text{--}850$  nm due to the presence of the “red edge,” and the reflectance near the red edge is strongly influenced by plant health.<sup>13)</sup> For vegetation evaluation, the normalized difference vegetation index (NDVI) is typically calculated using the reflectance of red and near-infrared region.<sup>14)</sup> Consequently, efficient near-infrared light sources have become increasingly important in the agricultural field. Although halogen lamps have been used as practical near-infrared light sources, their applications are limited due to high

power consumption, large size, short operating time, and high operating temperature. Therefore, the development of near-infrared emitting phosphors has been promoted to take advantage of phosphor-converted LEDs.<sup>15,16)</sup>

$\text{Cr}^{3+}$  is widely used as an activator in near-infrared phosphors because of its low cost and tunable emission bandwidth. Furthermore, its absorption bands extend from the ultraviolet (UV) to the blue region, enabling efficient excitation by UV or blue LEDs for the fabrication of phosphor-converted LEDs.<sup>17)</sup> It is probable that the  $\text{Cr}^{3+}$  prefers to occupy the six-coordinated octahedral site.<sup>18,19)</sup> Perovskite-type structure is suitable host material because of the six-coordinated octahedral site in its structures. Some  $\text{Cr}^{3+}$ -activated perovskite-type phosphor are reported such as  $\text{LaAlO}_3:\text{Cr}^{3+}$ ,<sup>20)</sup>  $\text{BaLaMgNbO}_6:\text{Cr}^{3+}$ ,<sup>21)</sup>  $\text{Ca}_2\text{AlNbO}_6:\text{Cr}^{3+}$ ,<sup>22)</sup> and  $\text{Sr}_2\text{AlTaO}_6:\text{Cr}^{3+}$ .<sup>23)</sup>  $\text{LaAlO}_3:\text{Cr}^{3+}$  exhibits sharp red emission peak at  $\sim 730$  nm, and potential for applying plant-growth LEDs, bio-imaging, and mechanoluminescence material.<sup>20,24,25)</sup> Škapin et al., reported that the perovskite-type structure was maintained in the solid solution of  $\text{La}_{1-x/3}\text{Al}_{1-x}\text{Ti}_x\text{O}_3$ .<sup>26)</sup> A-site deficiency of  $\text{La}^{3+}$  is introduced due to the charge compensation for  $\text{Ti}^{4+}$  doping to  $\text{Al}^{3+}$  of the B-site in the perovskite-type structure of  $\text{LaAlO}_3$ . In this study, the solid solution of  $\text{La}_{1-x/3}\text{Al}_{1-x}\text{Ti}_x\text{O}_3$  is focused as a host material. The luminescence properties depend on the crystal field strength around the activator of  $\text{Cr}^{3+}$ .<sup>17,21,22)</sup> In the perovskite-type  $\text{La}_{1-x/3}\text{Al}_{1-x}\text{Ti}_x\text{O}_3$  structure, the cation arrangement near the  $\text{Cr}^{3+}$  is changed, leading to a modification of the crystal field and enabling modulation of the luminescence properties. Therefore, we synthesized  $\text{Cr}^{3+}$ -activated  $\text{La}_{1-x/3}\text{Al}_{1-x}\text{Ti}_x\text{O}_3$  phosphors and investigated the optimal

<sup>†</sup> Corresponding author: A. Nakanishi; E-mail: NAKANISHI.Akihiro@nims.go.jp

<sup>‡</sup> Corresponding author: T. Takeda; E-mail: TAKEDA.Takashi@nims.go.jp

concentration of  $\text{Cr}^{3+}$ , luminescence property, quantum efficiency, and temperature-dependent luminescence. The effect of  $\text{Ti}^{4+}$  amounts to the temperature-dependent luminescence was revealed.

## 2. Experimental

$\text{La}_{1-x/3}\text{Al}_{1-x-y}\text{Ti}_x\text{O}_3:\text{yCr}^{3+}$  ( $x = 0.1-0.7$ ,  $\Delta x = 0.1$ ,  $y = 0.0015-0.05$ ) phosphors were synthesized by a solid-state reaction. Stoichiometric amounts of  $\text{La}_2\text{O}_3$  (99.99 %, Kojundo Chemical, Japan),  $\text{Al}_2\text{O}_3$  (99.99 %, TAIMEI CHEMICALS Co., LTD., Japan),  $\text{TiO}_2$  (99.9 %, Kojundo Chemical, Japan), and  $\text{Cr}_2\text{O}_3$  (99.9 %, Kojundo Chemical, Japan) were mixed thoroughly in an alumina mortar.  $\text{La}_2\text{O}_3$  was pre-heated at 800 °C for 10 h. After mixing, the precursor powder in the alumina crucible was calcined at 1500 or 1600 °C for 4 h in air.

The crystal phases of the synthesized powders were investigated at room temperature using powder X-ray diffraction (XRD, SmartLab X-ray Diffractometer, Rigaku, Japan) with  $\text{Cu-K}\alpha_1$  radiation at 45 kV, 200 mA, and  $2\theta$  in the range of 20–100°. The luminescence properties of powder samples were measured with a fluorescence spectrometer (FP-8600 spectrofluorometer, JASCO, Japan). The internal quantum efficiency (IQE) and external quantum efficiency (EQE) were measured by QE-2100 system (Otsuka Electronics, Japan).  $\text{BaSO}_4$  was used for references. The temperature-dependent luminescence properties were measured by a QE-2100 system combined with a temperature control stage (10002L, Rinkam Scientific Instruments, UK). The diffuse reflectance was measured in the range of 200–750 nm using UV-VIS-NIR spectrophotometer (UV-3600i Plus, SHIMADZU, Japan).

## 3. Results and discussion

In order to optimize the Ti amount in the  $\text{La}_{1-x/3}\text{Al}_{1-x-y}\text{Ti}_x\text{O}_3$  system,  $\text{La}_{1-x/3}\text{Al}_{1-x-y}\text{Ti}_x\text{O}_3:\text{yCr}^{3+}$  phosphors ( $x = 0.1-0.7$ ,  $\Delta x = 0.1$ ,  $y = 0.01$ ) were synthesized at 1500 °C for the preliminary experiment at first.  $\text{La}_{1-x/3}\text{Al}_{1-x-y}\text{Ti}_x\text{O}_3$  ( $x = 0.2$ ) was selected as the host material because the emission intensity peak around 750 nm was the highest under 365 nm excitation as shown in Fig. 1. In addition, the emission intensity of  $\text{La}_{1-x/3}\text{Al}_{1-x-y}\text{Ti}_x\text{O}_3$  ( $x = 0.2$ ,  $y = 0.01$ ) calcined at 1600 °C was higher than that of the sample calcined at 1500 °C. Based on the results of the preliminary experiment,  $\text{La}_{1-x/3}\text{Al}_{1-x-y}\text{Ti}_x\text{O}_3:\text{yCr}^{3+}$  ( $x = 0.2$ ,  $y = 0-0.05$ ) phosphors were synthesized at 1600 °C for 4 h. The XRD patterns of the  $\text{La}_{1-x/3}\text{Al}_{1-x-y}\text{Ti}_x\text{O}_3:\text{yCr}^{3+}$  ( $x = 0.2$ ,  $y = 0-0.05$ ) phosphors calcined at 1600 °C for 4 h are shown in Fig. 2. Diffraction patterns of all samples are consistent with the International Centre for Diffraction Data (ICDD) card peak patterns of  $\text{LaAlO}_3$  with the trigonal system (No. 00-030-1144),<sup>27)</sup> confirming the formation of single-phase phosphors. The cell volume of  $\text{La}_{1-x/3}\text{Al}_{1-x-y}\text{Ti}_x\text{O}_3:\text{yCr}^{3+}$  ( $x = 0.2$ ,  $y = 0, 0.01, 0.03$ , and 0.05) is shown in Fig. 3. With increasing the amount of  $\text{Cr}^{3+}$ , the cell volume expanded because the larger cation of  $\text{Cr}^{3+}$  ( $r^{\text{VI}} = 0.615 \text{ \AA}$ ) replaced the  $\text{Al}^{3+}$  ( $r^{\text{VI}} = 0.535 \text{ \AA}$ ) of the B-site in the perovskite-type structure.

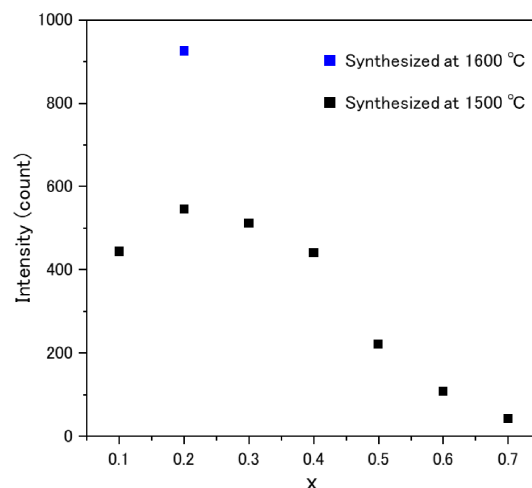


Fig. 1. Emission intensity under 365 nm excitation of  $\text{La}_{1-x/3}\text{Al}_{1-x-y}\text{Ti}_x\text{O}_3:\text{yCr}^{3+}$  ( $x = 0.1-0.7$ ,  $\Delta x = 0.1$ ,  $y = 0.01$ ) phosphors.

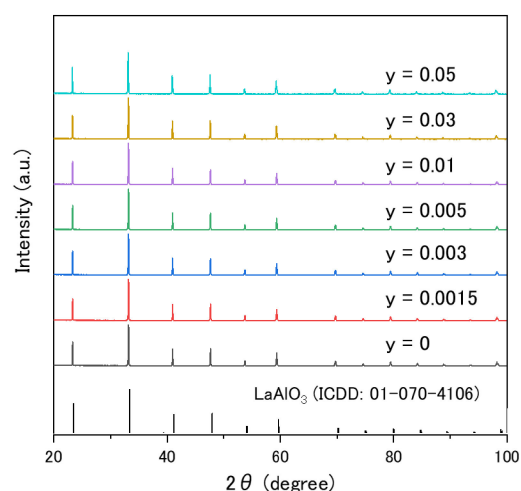


Fig. 2. XRD patterns of the  $\text{La}_{1-x/3}\text{Al}_{1-x-y}\text{Ti}_x\text{O}_3:\text{yCr}^{3+}$  ( $x = 0.2$ ,  $y = 0-0.05$ ) phosphors calcined at 1600 °C for 4 h.

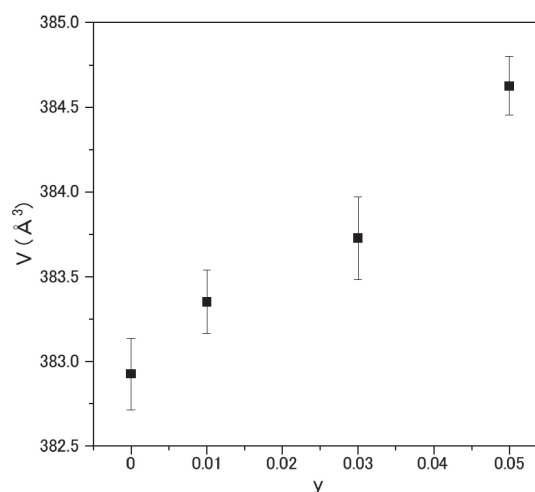
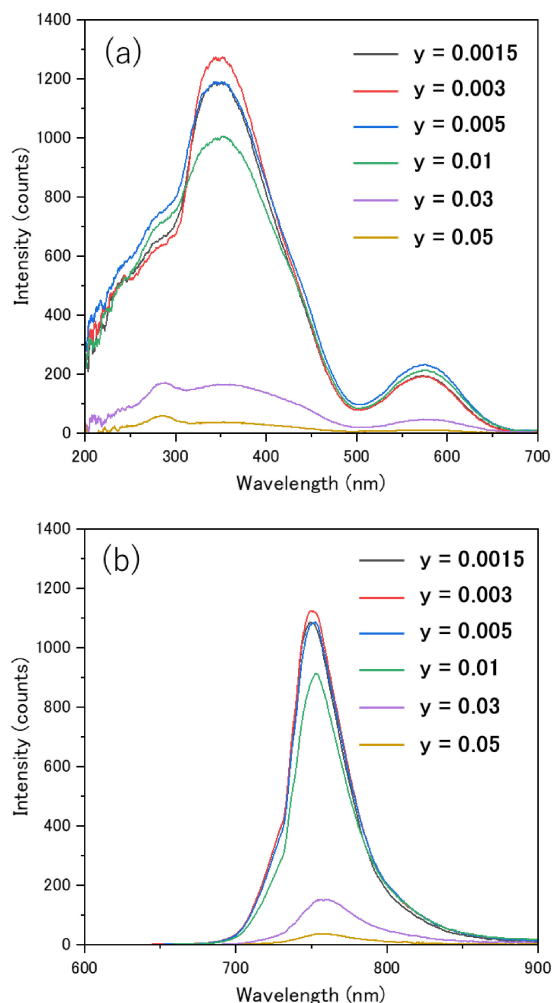


Fig. 3. Cell volume of  $\text{La}_{1-x/3}\text{Al}_{1-x-y}\text{Ti}_x\text{O}_3:\text{yCr}^{3+}$  ( $x = 0.2$ ,  $y = 0, 0.01, 0.03$ , and 0.05) phosphors calcined at 1600 °C for 4 h.



**Fig. 4.** (a) Excitation and (b) emission spectra of the  $\text{La}_{1-x/3}\text{Al}_{1-x-y}\text{Ti}_{3-y}\text{O}_3:\text{yCr}^{3+}$  ( $x = 0.2$ ,  $y = 0-0.05$ ) phosphors calcined at  $1600^\circ\text{C}$  for 4 h.

The excitation and emission spectra of the  $\text{La}_{1-x/3}\text{Al}_{1-x-y}\text{Ti}_{3-y}\text{O}_3:\text{yCr}^{3+}$  ( $x = 0.2$ ,  $y = 0-0.05$ ) phosphors calcined at  $1600^\circ\text{C}$  for 4 h are shown in **Figs. 4(a)** and **4(b)**. The sample with  $y = 0.003$  exhibited the highest emission intensity under 351 nm excitation. The emission intensity was rapidly decreasing after  $y = 0.01$  sample. The excitation spectra showed the absorption band peak around 350 and 570 nm, while the emission spectrum showed emission peak at 751 nm with a full width at half maximum (FWHM) of 41 nm in the sample with  $y = 0.003$ , originating from the d-d transition of  $\text{Cr}^{3+}$ . It is possible that the crystal field variation at the B-site of the perovskite-type  $\text{La}_{1-x/3}\text{Al}_{1-x}\text{Ti}_3\text{O}_3$  ( $x = 0.2$ ) affects the emission profile of  $\text{Cr}^{3+}$ .<sup>28)</sup>

The IQE, EQE, and absorbance of the  $\text{La}_{1-x/3}\text{Al}_{1-x-y}\text{Ti}_{3-y}\text{O}_3:\text{yCr}^{3+}$  ( $x = 0.1-0.3$ ,  $y = 0.003$ ) phosphors are summarized in **Fig. 5**. The excitation wavelengths for the samples with  $x = 0.1$ , 0.2, and 0.3 were set to 342, 351, and 354 nm, respectively, corresponding to their excitation peak. The IQE, EQE and absorbance of the sample with  $x = 0.1$ , 0.2, and 0.3 were 62.4, 21.3, and 34.1 % for  $x = 0.1$ ; 54.4, 25.5, and 47.0 % for  $x = 0.2$ ; and 38.9, 24.1,

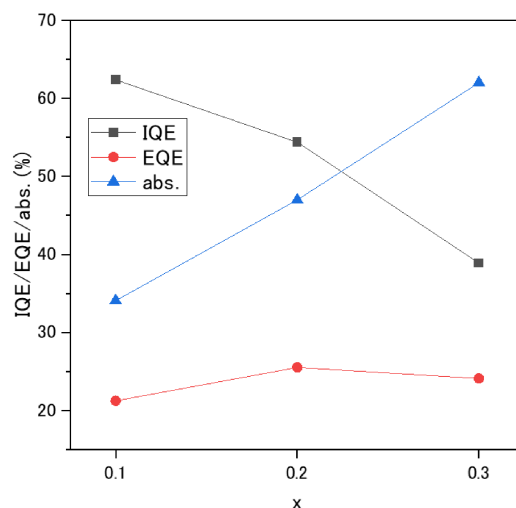


**Fig. 5.** IQE, EQE, and absorbance of the  $\text{La}_{1-x/3}\text{Al}_{1-x-y}\text{Ti}_3\text{O}_3:\text{yCr}^{3+}$  ( $x = 0.1-0.3$ ,  $y = 0.003$ ) phosphors calcined at  $1600^\circ\text{C}$  for 4 h.

and 62.0 % for  $x = 0.3$ , respectively. The highest value of the EQE was 25.5 % in the  $\text{La}_{1-x/3}\text{Al}_{1-x-y}\text{Ti}_3\text{O}_3:\text{yCr}^{3+}$  ( $x = 0.2$ ,  $y = 0.003$ ) phosphor. With increasing the value of  $x$ , the IQE was decreasing, while the absorbance was increasing.

The temperature-dependent luminescence intensity normalized by the room temperature value of the  $\text{La}_{1-x/3}\text{Al}_{1-x-y}\text{Ti}_3\text{O}_3:\text{yCr}^{3+}$  ( $x = 0.1-0.3$ ,  $y = 0.003$ ) phosphors are shown in **Fig. 6(a)**. The excitation wavelengths for the samples with  $x = 0.1$ , 0.2, and 0.3 were set to 342, 351, and 354 nm, respectively, corresponding to their excitation peak. The photoluminescence intensity gradually decreased with increasing the temperature in all samples due to the thermal quenching effect. The normalized intensities at  $150^\circ\text{C}$  of the sample with  $x = 0.1$ , 0.2, and 0.3 are 32, 17, and 3 %, respectively. The thermal quenching effect strongly occurred with increasing the amount of Ti. Ti content plays a crucial role in controlling the luminescence properties of  $\text{La}_{1-x/3}\text{Al}_{1-x-y}\text{Ti}_3\text{O}_3:\text{yCr}^{3+}$  ( $x = 0.1-0.3$ ,  $y = 0.003$ ) phosphors. Both IQE and the temperature at which the intensity drops 50 % of its room temperature intensity ( $T_{50}$ ) were also decreasing with increasing the amount of Ti. The diffuse reflectance of  $\text{La}_{1-x/3}\text{Al}_{1-x}\text{Ti}_3\text{O}_3$  ( $x = 0.1-0.3$ ) without  $\text{Cr}^{3+}$  doping is shown in **Fig. 6(b)**. In all samples, the absorbance edge was in the range of  $\sim 300$  nm. With increasing the value of  $x$ , the absorption edge was red shifted, indicating that the bandgap decreased.

It is probable that the thermal ionization effect occurs seriously in the more Ti-containing sample. Li et al. have reported  $\text{LaAlO}_3$  phosphors activated with  $\text{Mn}^{4+}$ , which has the same electron configuration as  $\text{Cr}^{3+}$ .  $\text{LaAlO}_3$  and  $\text{Ti}^{4+}$ -doped  $\text{LaAlO}_3$  were used as host materials. The conduction band of  $\text{Ti}^{4+}$ -doped  $\text{LaAlO}_3$  is shifted down compared with that of  $\text{LaAlO}_3$ , resulting in the enhancement of quenching due to the dissipation of excited electrons of  $\text{Mn}^{4+}$  into the conduction band.<sup>29)</sup> From the UV-vis diffuse reflectance measurement, it is confirmed that the band

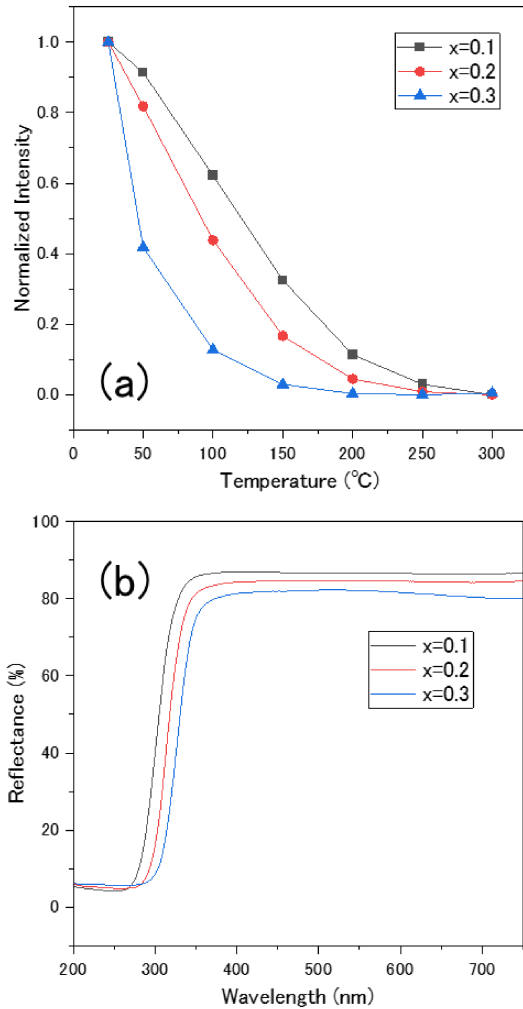


**Fig. 6.** (a) Emission intensity normalized by the room temperature value of the  $\text{La}_{1-x/3}\text{Al}_{1-x-y}\text{Ti}_3\text{O}_3:y\text{Cr}^{3+}$  ( $x = 0.1-0.3$ ,  $y = 0.003$ ) phosphors. (b) Diffuse reflectance spectra of  $\text{La}_{1-x/3}\text{Al}_{1-x-y}\text{Ti}_3\text{O}_3$  ( $x = 0.1-0.3$ ) without  $\text{Cr}^{3+}$  doping.

gap of the host material  $\text{La}_{1-x/3}\text{Al}_{1-x}\text{Ti}_3\text{O}_3$  ( $x = 0.1-0.3$ ) decreased with increasing the amount of Ti, indicating that the thermal quenching is caused due to the thermal ionization effect.<sup>30)</sup> On the other hand, the absorbance (as shown in Fig. 5) was linearly increasing with increasing the amount of Ti although the amount of Cr doping was fixed at  $y = 0.003$ . It is possible that the local coordination environment around  $\text{Cr}^{3+}$  is modulated by the  $\text{Ti}^{4+}$  doping, resulting in the absorption enhancement. Liang et al. have reported that the emission intensity of  $\text{Mg}_{14}\text{Ge}_5\text{O}_{24}:\text{Mn}^{4+}$  phosphor was enhanced by  $\text{Ti}^{4+}$  doping to the host material.<sup>31)</sup> Lingling et al. investigated the effect of  $\text{Ti}^{4+}$  doping to  $\text{SrGe}_4\text{O}_9:\text{Mn}^{4+}$  phosphor.  $\text{Ti}^{4+}$  doping improved the emission intensity because of the modification of the coordination environment around  $\text{Mn}^{4+}$ .<sup>32)</sup> However, the absorption enhancement and thermal quenching behavior exhibit a trade-off relationship in the  $\text{La}_{1-x/3}\text{Al}_{1-x-y}\text{Ti}_3\text{O}_3:y\text{Cr}^{3+}$  ( $x = 0.1-0.3$ ,  $y = 0.003$ ) phosphors. Therefore, fine-tuning the Ti content within the range of  $x = 0.1-0.3$  is necessary to optimize the luminescence properties in future studies.

**Table 1.** Luminescence properties of  $\text{Cr}^{3+}$ -activated phosphors with the perovskite-type structure

Host	$\lambda_{\text{ex}}$ (nm)	$\lambda_{\text{em}}$ (nm)	FWHM (nm)	IQE (%)	EQE (%)	$I_{150^\circ\text{C}}$ (%)	Ref.
$\text{Ca}_2\text{AlNbO}_6$	337	744	49	32.6		54	22)
$\text{Sr}_2\text{AlTaO}_6$	303	704	36				23)
$\text{Sr}_2\text{AlNbO}_6$	323	760	34*	66.1	28.4	52	33)
$\text{La}_2\text{MgTiO}_6$	349	766	59*	21.6		41.7	34)
<b><math>\text{La-Al-Ti-O}</math> (<math>x = 0.2</math>)</b>	<b>351</b>	<b>751</b>	<b>41</b>	<b>54.4</b>	<b>25.5</b>	<b>17</b>	<b>This study</b>

\*As the value was not shown in the paper, it was read from the emission spectrum.

**Table 1** shows the luminescence properties of  $\text{Cr}^{3+}$ -activated phosphor with the perovskite-type structure.<sup>22,23,33,34)</sup> The excitation peak of the  $x = 0.2$  sample is 351 nm, which is the closest to UV 365 nm LEDs. The IQE and EQE are also comparable to others, while the photoluminescence intensity at 150 °C is the lowest. The temperature-dependence luminescence property should be improved by the adjustment of the Ti content of host material  $\text{La}_{1-x/3}\text{Al}_{1-x-y}\text{Ti}_3\text{O}_3$ . In summary, the  $\text{La}_{1-x/3}\text{Al}_{1-x-y}\text{Ti}_3\text{O}_3:y\text{Cr}^{3+}$  phosphor exhibits near-infrared emission under UV excitation and thus has potential applications as a near-infrared phosphor in the plant-growth or sensing technologies.

#### 4. Conclusion

Near-infrared emitting phosphor  $\text{La}_{1-x/3}\text{Al}_{1-x-y}\text{Ti}_3\text{O}_3:y\text{Cr}^{3+}$  were successfully synthesized by a solid-state reaction for use in the plant-growth or remote sensing application.  $\text{La}_{1-x/3}\text{Al}_{1-x-y}\text{Ti}_3\text{O}_3:y\text{Cr}^{3+}$  ( $x = 0.2$ ,  $y = 0.003$ ) phosphor exhibited near-infrared emission at 751 nm with a FWHM of 41 nm under UV excitation, indicating the possibility of applying for the near-infrared emitting LED with UV LED chip. The IQE and EQE were 54.4 and 25.5 %, respectively. This infrared phosphor targeting the plant leaf red-edge region ( $\sim 750$  nm) was developed by  $\text{Ti}^{4+}$  doping of a  $\text{LaAlO}_3$  host material. The emission peak is red-shifted relative to that of  $\text{LaAlO}_3:\text{Cr}^{3+}$  phosphor as a result of tuning the local coordination environment around the  $\text{Cr}^{3+}$  activator. Notably, the IQE under UV excitation is the highest among the Al-containing  $\text{Cr}^{3+}$ -activated infrared phosphors, such as  $\text{Ca}_2\text{AlNbO}_6:\text{Cr}^{3+}$  and  $\text{Sr}_2\text{AlNbO}_6:\text{Cr}^{3+}$ . The temperature-dependence luminescence and the diffuse reflectance measurement revealed that Ti amount plays a crucial role in controlling the thermal quenching behavior of  $\text{La}_{1-x/3}\text{Al}_{1-x-y}\text{Ti}_3\text{O}_3:y\text{Cr}^{3+}$  ( $x = 0.1-0.3$ ,  $y = 0.003$ ) phosphors. This study provides a development strategy for  $\text{Cr}^{3+}$ -activated near-infrared emitting phosphors.

**Acknowledgments** This work was supported by Innovative Science and Technology Initiative for Security (Grant Number JPJ004596, ATLA, Japan).

#### References

- 1) E. F. Schubert and J. K. Kim, *Science* 308, 1274 (2005).
- 2) C. J. Humphreys, *MRS Bull.* 33, 459 (2008).

- 3) C. C. Lin and R.-S. Liu, *J. Phys. Chem. Lett.* **2**, 1268 (2011).
- 4) Z. Xia and A. Meijerink, *Chem. Soc. Rev.* **46**, 275 (2017).
- 5) R.-J. Xie, N. Hirotsaki, K. Sakuma, Y. Yamamoto and M. Mitomo, *Appl. Phys. Lett.* **84**, 5404 (2004).
- 6) K.-B. Kim, Y.-I. Kim, H.-G. Chun, T.-Y. Cho, J.-S. Jung and J.-G. Kang, *Chem. Mater.* **14**, 5045 (2002).
- 7) K. Uheda, N. Hirotsaki, Y. Yamamoto, A. Naito, T. Nakajima and H. Yamamoto, *Electrochem. Solid St.* **9**, H22 (2006).
- 8) Y. Q. Li, J. E. J. van Steen, J. W. H. van Krevel, G. Botty, A. C. A. Delsing, F. J. Disalvo, G. de With and H. T. Hintzen, *J. Alloy. Compd.* **417**, 273 (2006).
- 9) X. Yang, Y. Zhang, X. Zhang, J. Chen, H. Huang, D. Wang, X. Chai, G. Xie, M. S. Molokeev, H. Zhang, Y. Liu and B. Lei, *J. Am. Ceram. Soc.* **103**, 1773 (2020).
- 10) W. Wu, Z. Zhang, R. Dong, G. Xie, J. Zhou, K. Wu, H. Zhang, Q. Cai and B. Lei, *J. Rare Earth.* **38**, 539 (2020).
- 11) Z. Ren, H. Yu, J. Zhang, X. Li, S. Xu and B. Chen, *Inorg. Chem.* **63**, 21155 (2024).
- 12) M.-H. Fang, G. N. A. De Guzman, Z. Bao, N. Majewska, S. Mahlik, M. Grinberg, G. Leniec, S. M. Kaczmarek, C.-W. Yang, K.-M. Lu, H.-S. Sheu, S.-F. Hu and R.-S. Liu, *J. Mater. Chem. C* **8**, 11013 (2020).
- 13) D. Al-Shammari, B. M. Whelan, C. Wang, R. G. V. Bramley and T. F. A. Bishop, *Eur. J. Agron.* **164**, 127479 (2025).
- 14) S. Amani and H. Shafizadeh-Moghadam, *Agr. Water Manage.* **284**, 108324 (2023).
- 15) H. Lee, S. Cho, J. Lim, A. Lee, S.-W. Chun, M.-J. Kim and C. Mo, *Sensors* **23**, 1961 (2023).
- 16) S. Chen, M. Han, J. Li, Y. Li, Z. Gao, Y. Zhang, M. Meng, Q. Zhang, D. Deng and L. Chen, *Ceram. Int.* **49**, 36360 (2023).
- 17) C. Chen, J. Chang, R. Chen, R. Gao, Y. Wang, K. Zhu, J. Xiang and C. Guo, *Mater. Chem. Front.* **9**, 1821 (2025).
- 18) P. J. Dereń, M. Malinowski and W. Stręk, *J. Lumin.* **68**, 91 (1996).
- 19) J. Lai, J. Zhou, Z. Long, J. Qiu, D. Zhou, Y. Yang, K. Zhang, W. Shen and Q. Wang, *Mater. Design* **192**, 108701 (2020).
- 20) Y. Katayama, H. Kobayashi and S. Tanabe, *Appl. Phys. Express* **8**, 012102 (2015).
- 21) Y. Wang, Y. Sun, Z. Xu, X. Xing and M. Shang, *Inorg. Chem.* **63**, 8899 (2024).
- 22) H. Gao, B. Devakumar and X. Huang, *Ceram. Int.* **51**, 8321 (2025).
- 23) M. Han, S. Chen, J. Li, Z. Gao, Y. Zhang, Y. Shen, Y. Tian and D. Deng, *J. Alloy. Compd.* **973**, 172927 (2024).
- 24) K. T. Thu, N. Tu, D. Q. Trung, N. V. Du, M. T. Tran, N. V. Quang, T. N. Bach, N. T. H. Lien, N. D. Hung, D. X. Viet, N. D. T. Kien and P. T. Huy, *Ceram. Int.* **50**, 27064 (2024).
- 25) P. Shao, P. Xiong, Y. Xiao, Z. Chen, D. Chen and Z. Yang, *Adv. Powder Technol.* **3**, 100165 (2024).
- 26) S. Škapin, D. Kolar and D. Suvorov, *J. Am. Ceram. Soc.* **76**, 2359 (1993).
- 27) J. Zhao, N. L. Ross and R. J. Angel, *J. Phys.-Condens. Mat.* **16**, 8763 (2004).
- 28) C. Chen, J. Chang, R. Chen, R. Gao, Y. Wang, K. Zhu, J. Xiang and C. Guo, *Mater. Chem. Front.* **9**, 1821 (2025).
- 29) S. Li, C. Zhang, Q. Zhu and J.-G. Li, *Inorg. Chem. Front.* **10**, 638 (2023).
- 30) J. Ueda, S. Tanabe and T. Nakanishi, *J. Appl. Phys.* **110**, 053102 (2011).
- 31) S. Liang, G. Li, P. Dang, Y. Wei, H. Lian and J. Lin, *Adv. Opt. Mater.* **7**, 1900093 (2011).
- 32) P. Lingling, C. Shixiu, Q. Qinpeng, D. Ying, C. Wenbo, H. Tao and L. Bitao, *Adv. Opt. Mater.* **7**, 1900093 (2011).
- 33) Z. Liu, Y. Tang, X. Zhang, N. Pan, H. Shi, P. Lyu, C. Xu and L. Sun, *Ceram. Int.* **51**, 26645 (2025).
- 34) P.-X. Gao, P. Dong, Z.-Y. Zhou, X.-J. Zhang, Y.-N. Li, J.-K. Yang, Q. Li, K. Chen, M. S. Molokeev, Z. Zhou and M. Xia, *Chin. J. Lumin.* **43**, 58 (2022).